

Sensitivity to neutrino mixing parameters with atmospheric neutrinos

Abhijit Samanta *

Harish-Chandra Research Institute, Chhatnag Road, Jhusi, Allahabad 211 019, India

(Dated: November 20, 2018)

We have analyzed the atmospheric neutrino data to study the octant of θ_{23} and the precision of the oscillation parameters for a large Iron CALorimeter (ICAL) detector. The ICAL being a tracking detector has the ability to measure the energy and the direction of the muon with high resolution. From bending of the track in magnetic field it can also distinguish its charge. We have generated events by Nuance and then considered only the muons (directly measurable quantities) produced in charge current interactions in our analysis. This encounters the main problem of wide resolutions of energy and baseline. The energy-angle correlated two dimensional resolution functions are used to migrate the energy and the zenith angle of the neutrino to those of the muon. A new type of binning has been introduced to get better reflection of the oscillation pattern in chi-square analysis. Then the marginalization of the χ^2 over all parameters has been carried out for neutrinos and anti-neutrinos separately. We find that the measurement of θ_{13} is possible at a significant precision with atmospheric neutrinos. The precisions of Δm_{32}^2 and $\sin^2 \theta_{23}$ are found $\sim 8\%$ and 38% , respectively, at 90% CL. The discrimination of the octant as well as the deviation from maximal mixing of atmospheric neutrinos are also possible for some combinations of $(\theta_{23}, \theta_{13})$. We also discuss the impact of the events at near horizon on the precision studies.

PACS numbers: 14.60.Pq

I. INTRODUCTION

Recent discovery of the neutrino mass has opened up a new window into physics beyond the standard model. Aside from this fact, the two surprising sets of results [1], i) the extremely small masses of neutrinos (very different from quark sector) and ii) a dramatically different mixing pattern from quarks, indicate a new direction of this field. The first one may be the hint of a new symmetry such as $B - L$ at high scales so that one can use a mechanism like seesaw to resolve the puzzle of the smallness of the masses. On the other hand, the second one poses a much more challenging problem. One can expect a new symmetry for leptons as well as for quarks to solve this problem. Currently, there are many theoretical ideas. For example, the $\mu - \tau$ symmetry [2] is invoked to explain the maximal mixing. However, if this $\mu - \tau$ symmetry exists, it leads to $\delta_{CP} = 0$ and $\theta_{13} = 0$. It should be broken if there appears a nonzero θ_{13} and CP violation. In that case the octant (the sign of $\theta_{23} - 45^\circ$) and the nonzero value of θ_{13} emerges other new possibilities. It is also expected that neutrino theories may have implications on the very fascinating fields like observed

matter-antimatter asymmetry of the universe, grand unification, supersymmetry, extra dimensions, etc[3].

Active endeavors are under way to launch the era of precision experiments with a thrust to uncover the underlying principle that gives neutrino masses and their mixing. This is one of the most promising ways to explore physics beyond the standard model. In the standard oscillation picture there are six parameters. The present 1σ , 2σ and 3σ confidence level (CL) ranges from global 3ν oscillation analysis (2008) [1] are very exciting (see table I). Recently, new bounds, $\theta_{13} = -0.07_{-0.11}^{+0.18}$ and the asymmetry $\theta_{23} - \pi/4 = 0.03_{-0.15}^{+0.09}$ at 90% CL have been shown in [4, 5] from an analysis considering all present neutrino data. The CP-violating phase δ_{CP} is still unconstrained.

Despite of these spectacular achievements, a lot of things are still missing. Tremendous efforts are underway to determine the mass ordering (sign of Δm_{32}^2), the values of θ_{13} and δ_{CP} , and to discriminate the octant degeneracy of θ_{23} in future experiments. We define $\Delta m_{32}^2 = m_3^2 - m_2^2$. There are many ongoing and planned experiments: UNO [6], T2K [7], NOvA [8], Hyper-Kamiokande [9], INO [10] and many others. The main characteristic feature of a magnetized Iron CALorimeter (ICAL) detector proposed at India-based Neutrino Observatory (INO) is that it has the capability to detect ν_μ and $\bar{\nu}_\mu$ separately, which measures directly the matter effect.

*E-mail address: abhijit@hri.res.in

Parameter	$\Delta m_{21}^2/10^{-5} \text{ eV}^2$	$\sin^2 \theta_{12}$	$\sin^2 \theta_{13}$	$\sin^2 \theta_{23}$	$ \Delta m_{31}^2 /10^{-3} \text{ eV}^2$
Best fit	7.67	0.312	0.016	0.466	2.39
1σ range	7.48 – 7.83	0.294 – 0.331	0.006 – 0.026	0.408 – 0.539	2.31 – 2.50
2σ range	7.31 – 8.01	0.278 – 0.352	< 0.036	0.366 – 0.602	2.19 – 2.66
3σ range	7.14 – 8.19	0.263 – 0.375	< 0.046	0.331 – 0.644	2.06 – 2.81

TABLE I: Global 3ν oscillation analysis (2008)

Unlike a fixed baseline neutrino beam experiment, the atmospheric neutrino flux covers a wide range of baseline (a few km – 12900 km) and energy (sub GeV – a few hundred GeV). On the other hand, it is not known well and there are huge uncertainties in its estimation. It is also a very rapidly falling function of energy. So, the extraction of the results from the experimental data is very complicated.

The deviation from maximal mixing and the discrimination of octant degeneracy of θ_{23} have been studied in [11, 12] with atmospheric neutrinos for a large magnetized ICAL detector. However, the results have been obtained without marginalization and assuming the Gaussian resolution functions of fixed widths for whole range of energy and zenith angle. The energy range for the atmospheric neutrinos is very wide. The resolutions are changed significantly over its range and are very different for neutrinos and anti-neutrinos. Moreover, the energy resolutions appear to be non-Gaussian due to some unmeasurable product particles like neutral hadrons in neutrino interaction even if one considers all visible hadrons.

For a given neutrino energy and direction, there is a distribution in the reconstructed energy and direction. Again, a particular reconstructed energy and direction can come from a wide range of true neutrino energy and direction. So, it is not possible to convert a distribution in reconstructed energy and direction obtained from an experiment to a distribution in actual neutrino energy and direction. This restricts the binning of the data for chi-square analysis only in experimentally measured energy and direction. On the other hand, the actual resolution functions have no regular pattern and significantly deviate from the Gaussian nature even if we consider the visible hadrons. Again, the width changes with neutrino energy. For a simplistic analysis, if one considers a Gaussian resolution with a width that gives equal space under the surface of resolution function, the correct theoretical data smearing this approximated Gaussian resolution function can not be obtained for chi-square analysis. As a consequence, the best-fits and the contours of oscillation

parameters will differ largely from the true values. In literature, there are many analyses where both the theoretical as well as the experimental data are obtained by smearing the Gaussian resolution functions. For an example, see ref. [12]. However, the result changes very rapidly with change of the width of the resolution. So, realistic estimation of the capability of an experiment can be done only by an analysis with experimentally measurable quantities and exact resolution functions.

Till now, the precision studies with atmospheric neutrinos have mainly carried out for water Cherenkov detector, a non-magnetized detector. It is very important to see the capability of a large magnetized detector. We have studied the neutrino oscillation considering neutrinos and anti-neutrinos separately in the chi-square analysis. Here, we consider the muons (directly measurable quantities at ICAL) produced by the charge current interactions. We generate events by Nuance-v3 [13]. The two dimensional energy-angle correlated resolution functions are used to migrate the energy and the zenith angle of the neutrino to the energy and the zenith angle of the muon.

The above method has been introduced in [14] and later used in [15]. The goal of the previous work [15] was only to compare the allowed parameter space of oscillation parameters obtained from different types of binning. The considered systematic uncertainties were very much different from the present systematic uncertainties. The purpose of this work is to study the following.

We consider whole data set in previous studies. But in reality, the horizontal events cannot be detected when the iron slabs are stacked horizontally. In this paper, we have studied the impact of these events in determining the precision of the parameters with and without considering a rejection criteria for the horizontal events. This is very crucial to determine whether horizontal stacking of iron plates is better than the vertical stacking or not.

As discussed in [15], the binning of the data neither in $\log E - \cos \theta_{\text{zenith}}$ nor in $\log E - \log L$ is the optimum. In this paper, we have optimized the binning in L . These

are equal binned grids in $\log E - L^{0.4}$ plane, which can capture the oscillation behavior for all L and E in a better way in the chi-square analysis. Again, the number of bins in both axes need optimization between resolutions and statistics. However, it should be noted here that if the statistics is huge for whole range of E and L , one can solve this problem by making the bin size very small and then the type of binning will not play any crucial role. However, the type of binning is very crucial when the analyses is in experimentally measurable energy and directions. Here the statistics over measured energy and direction is redistributed notably from the true neutrino energy and direction.

Finally, we have made a detailed study on the sensitivity of a magnetized ICAL detector in determining the precision of Δm_{32}^2 and θ_{13} as well as in discriminating the octant ambiguity of θ_{23} . We find the sensitivities of the parameters in two dimensional parameter space after marginalization over whole allowed ranges of the parameters. The absolute bounds of each parameter are also studied.

II. ATMOSPHERIC NEUTRINO FLUX AND EVENTS

The atmospheric neutrinos are produced by the interactions of the cosmic rays mainly with nucleuses of molecules in the earth's atmosphere. The knowledge of primary spectrum of the cosmic rays has been improved from the observations by BESS[16] and AMS[17]. However, large regions of parameter space have not been explored and they are interpolated or extrapolated from the measured flux. The difficulties and the uncertainties in the calculation of the neutrino flux depend on the neutrino energy. The low energy fluxes have been known quite well. The cosmic ray fluxes (< 10 GeV) are modulated by the solar activity and the geomagnetic field through a rigidity (momentum/charge) cutoff. At the higher neutrino energy (> 100 GeV), the solar activity and the rigidity cutoff are irrelevant[18]. There is 10% agreement among the calculations for neutrino energy below 10 GeV because different hadronic interaction models are used in the calculations and because the uncertainty in the cosmic ray flux measurement is 5% for the cosmic ray energy below 100 GeV [18]. In our simulation, we have used a typical Honda flux calculated in 3-dimensional scheme[18].

The interactions of neutrinos with the detector mate-

rial are simulated using the Monte Carlo model Nuance (version-3)[13]. Here, the charged current (CC) and neutral current (NC) interactions are considered for (quasi-)elastic, resonance, coherent, diffractive, and deep inelastic scattering processes.

III. OSCILLATION OF ATMOSPHERIC NEUTRINOS

The present atmospheric neutrino data are well explained by two flavor oscillation [19, 20]. However, one expects a considerable $\nu_\mu \rightarrow \nu_e$ oscillation of atmospheric neutrinos in 3-flavor framework if θ_{13} is nonzero. To understand the analytical solution one may adopt the so called "one mass scale dominance" (OMSD) framework: $|\Delta m_{21}^2| \ll |m_3^2 - m_{1,2}^2|$. Then the oscillation probabilities can be expressed as:

$$\begin{aligned} P_{\mu e} &= P_{e\mu} \\ &= \sin^2 \theta_{23} \sin^2 2\theta_{13} \sin^2 \left(\frac{1.27 \Delta m_{31}^2 L}{E} \right); \\ P_{\mu\mu} &= 1 \\ &\quad - 4 \cos^2 \theta_{13} \sin^2 \theta_{23} (1 - \cos^2 \theta_{13} \sin^2 \theta_{23}) \\ &\quad \times \sin^2 \left(\frac{1.27 \Delta m_{31}^2 L}{E} \right). \end{aligned} \quad (1)$$

These oscillation probabilities are derived for vacuum. Since the oscillation involves electron neutrino, it will be modulated by the matter effect [21, 22]. Then,

$$\begin{aligned} P_{\mu e}^m &= P_{e\mu}^m \\ &= \sin^2 \theta_{23} \sin^2 2\theta_{13}^m \sin^2 \left(\frac{1.27 \Delta (m_{31}^2)^m L}{E} \right). \end{aligned} \quad (2)$$

Here, E , L and Δm_{31}^2 are in GeV, km and eV^2 , respectively.

$$\begin{aligned} P_{\mu\mu}^m &= 1 - \cos^2 \theta_{13}^m \sin^2 2\theta_{23} \\ &\quad \times \sin^2 \left[1.27 \left(\frac{(\Delta m_{31}^2)^m + A + (\Delta m_{31}^2)^m}{2} \right) \frac{L}{E} \right] \\ &\quad - \sin^2 \theta_{13}^m \sin^2 2\theta_{23} \\ &\quad \times \sin^2 \left[1.27 \left(\frac{(\Delta m_{31}^2)^m + A - (\Delta m_{31}^2)^m}{2} \right) \frac{L}{E} \right] \\ &\quad - \sin^4 \theta_{23} \sin^2 2\theta_{13}^m \sin^2 \left[1.27 (\Delta m_{31}^2)^m \frac{L}{E} \right] \end{aligned} \quad (3)$$

The mass squared difference $(\Delta m_{31}^2)^m$ and mixing angle $\sin^2 2\theta_{13}^m$ in matter are related to their vacuum values

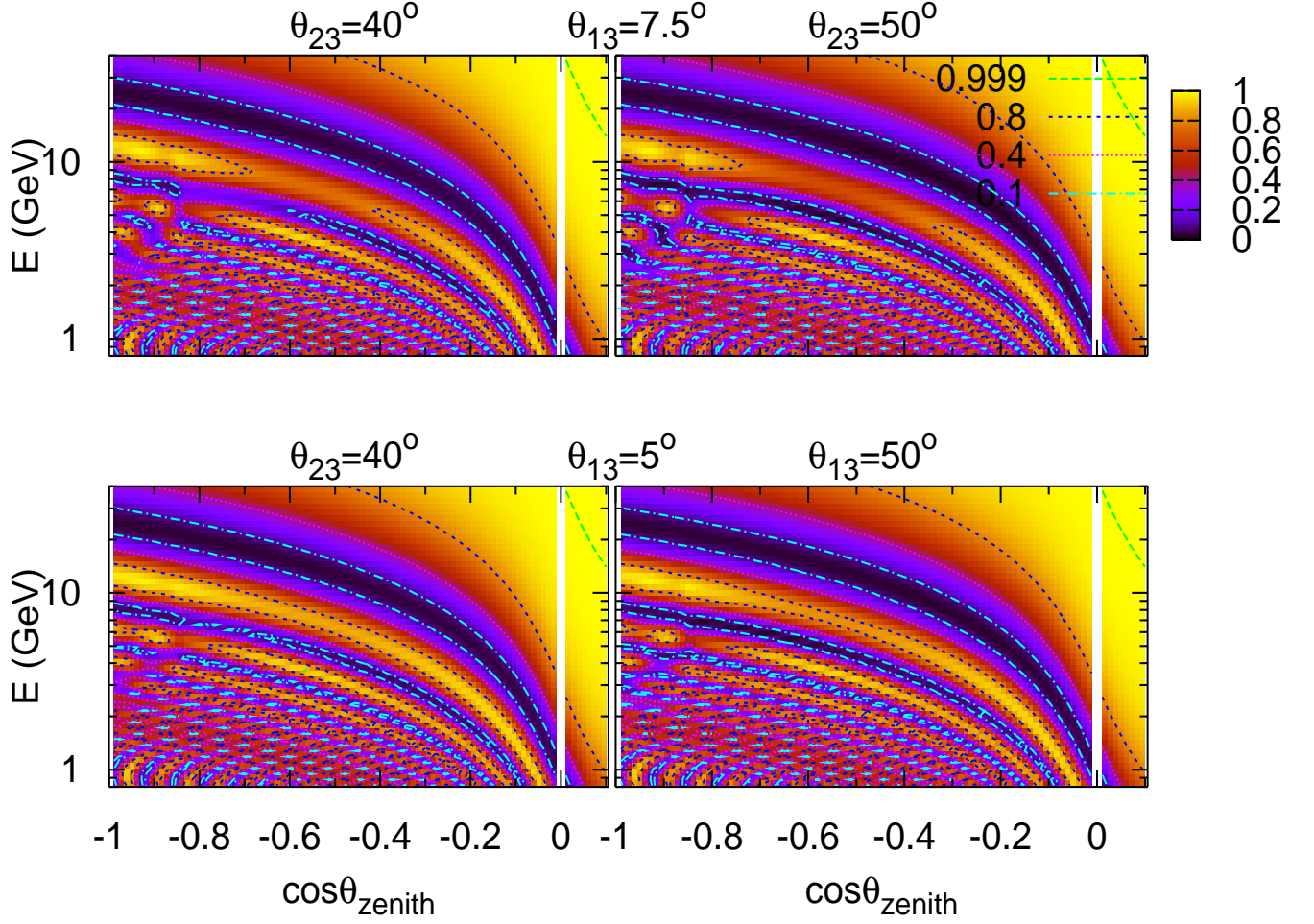


FIG. 1: The oscillogram of $\bar{\nu}_\mu \rightarrow \bar{\nu}_\mu$ oscillation probability in $E - \cos\theta_{\text{zenith}}$ plane for $\theta_{23} = 40^\circ$ (left column) and 50° (right column) with $\theta_{13} = 5^\circ$ (lower row) and 7.5° (upper row). We choose $\Delta m_{32}^2 = -2.5 \times 10^{-3} \text{eV}^2$ and $\delta_{CP} = 0$.

by

$$(\Delta m_{31}^2)^m = \sqrt{((\Delta m_{31}^2) \cos 2\theta_{13} - A)^2 + ((\Delta m_{31}^2) \sin 2\theta_{13})^2}, \quad (\text{IH}) \quad \text{when} \quad \sin^2 2\theta_{13}^m \rightarrow 1 \quad \text{or,} \quad A = \Delta m_{31}^2 \cos 2\theta_{13}. \quad (5)$$

$$\sin 2\theta_{13}^m = \frac{(\Delta m_{31}^2) \sin 2\theta_{13}}{\sqrt{((\Delta m_{31}^2) \cos 2\theta_{13} - A)^2 + ((\Delta m_{31}^2) \sin 2\theta_{13})^2}}, \quad (4)$$

where, $A = 2\sqrt{2}G_F N_e E$, G_F is the Fermi constant, N_e is the electron density of the medium and E is neutrino energy [23]. The matter potential term A has the same absolute value, but opposite sign for neutrino and anti-neutrino. The superscript ‘m’ denotes effective parameters in matter. Due to this matter effect, the Mikheyev-Smirnov-Wolfenstein (MSW) resonance occurs in $P(\nu_\mu \rightarrow \nu_e)$ or $P(\nu_e \rightarrow \nu_\mu)$. It happens for Normal Hierarchy (NH) with neutrinos and for Inverted Hierarchy (IH) with anti-neutrinos. It can be understood from Eq.

3 and 4 that a resonance in above oscillation probabilities will occur for neutrinos (anti-neutrinos) with NH

Then the resonance energy can be expressed as

$$E = \left[\frac{1}{2 \times 0.76 \times 10^{-4} Y_e} \right] \left[\frac{|\Delta m_{31}^2|}{\text{eV}^2} \cos 2\theta_{13} \right] \left[\frac{\text{gm/cc}}{\rho} \right]. \quad (6)$$

The resonance energy corresponding to a baseline can be seen in [14].

The oscillogram of muon survival probability is demonstrated in Fig. 1 for $\theta_{13} = 5^\circ$ and 7.5° with $\theta_{23} = 40^\circ$ and 50° , respectively. Here, we show the resonance ranges for the neutrinos passing through the core of the earth (with $E \approx 3 - 6 \text{ GeV}$) and the mantle of the earth (with

$E \approx 5 - 10$ GeV). We also see a difference for $\theta_{23} = 40^\circ$ and 50° due to the $\sin^4 \theta_{23}$ term (Eq. 3), which dominates over the other terms due to the matter effect.

IV. BINNING OF THE EVENTS

For binning of the data in E , we need to consider the following facts. I) The atmospheric neutrino flux falls very rapidly with increase in energy. II) Again, the wide resolutions of E and L between true neutrinos and reconstructed neutrinos smear the oscillation effect to a significant extent. The wide resolutions arise mainly due to the interaction kinematics. This huge uncertainty in reconstructed neutrino momentum is due to the un-observable product particles and slightly due to the un-measurable momentum of recoiled nucleus when $E \lesssim 1$ GeV. For this reason, the energy resolutions deviate largely from the Gaussian nature. These are strongly neutrino energy dependent. At low energy ($E \lesssim 1.5$ GeV) the quasi-elastic process dominates and the muon carries almost whole energy of the neutrino. The energy resolution is very good here. With increase in energy, the width of the resolution increases significantly as the deep inelastic event dominates as well as the flux also falls very rapidly. This is one of the main problems in the atmospheric neutrino experiments. III) There is also an important characteristics of the oscillation probability when both L and E are varied simultaneously. We explain it here for $\nu_\mu \leftrightarrow \nu_\mu$ oscillation in vacuum, which is a sinusoidal function of L/E . If we plot it in $L - E$ plane (see Fig. 2), it is seen that the distance between two consecutive peaks of oscillation in E for a fixed L increases very rapidly with E . These three points suggest increase in bin size with increase in E . We choose equal bin size in $\log E$.

Again, the distance between two consecutive peaks of oscillation in L for a fixed E increases rapidly as we go to lower values of L . When this distance is very small compared to the resolution width of L , the oscillation effect is averaged out. Only when the distance is large, it contributes to oscillation measurements. To get the reflection of this oscillation pattern in χ^2 , we need decreasing bin size of L with decreasing of its value. This has been studied in detail for three common choices of binning of the data in [15], and it has been found that neither $\log E - \cos \theta_{\text{zenith}}$ nor in $\log E - \log L$ is optimum. In this work we optimize the binning the data in the grids of $\log E - L^{0.4}$ plane.

The number of bins used for this analysis is discussed

later in the section VI. Here, it should be noted that one cannot make the bin size arbitrarily small. The number of event in a bin may be a fraction of 1 in theoretical data for chi-square analysis, but the number of event in experimental data is either zero or integer number greater or equal to 1. Obviously, no chi-square method will work if many of the bins have number of event equal to zero or just equal to 1. However, the number of events per bin ≥ 1 is not also sufficient. We have checked that one needs number of event per bin at least > 4 to obtain $\chi^2/\text{d.o.f} \approx 1$. This indicates the optimization of bin size with statistics.

V. SELECTION OF EVENTS

The up going and down going events are mixed at the near horizon due the uncertainty in scattering angle between neutrino and muon. The up going neutrinos get oscillated and down going neutrinos remain almost unoscillated due to the short distance from the source to the detector. When the iron plates of ICAL detector are placed horizontally, all these events cannot be detected. The high energy events will have normally small scattering angle, but very long tracks in the detector. So, they may be detected. If we plot the distribution of the difference in zenith angles between neutrino and the corresponding muon for a fixed energy, it gives a Gaussian plot. The half width at the half maxima of this distribution as a function of muon energy is shown in fig 3. We put a selection criteria that the events for a given muon energy having the difference $|90^\circ - \theta_{\text{zenith}}|$ within the above half width are rejected. Here we expect roughly that these events cannot be detected in case of real experiments. The precisions determined with and without this cut is discussed later.

VI. THE χ^2

The number of events falls very rapidly with increase in energy and there is a very small statistics at the high energy. However, the contributions to the sensitivities of the oscillation parameters is significant from these high energy events. For the low statistics at the high energy, the χ^2 is calculated according to the Poisson probability

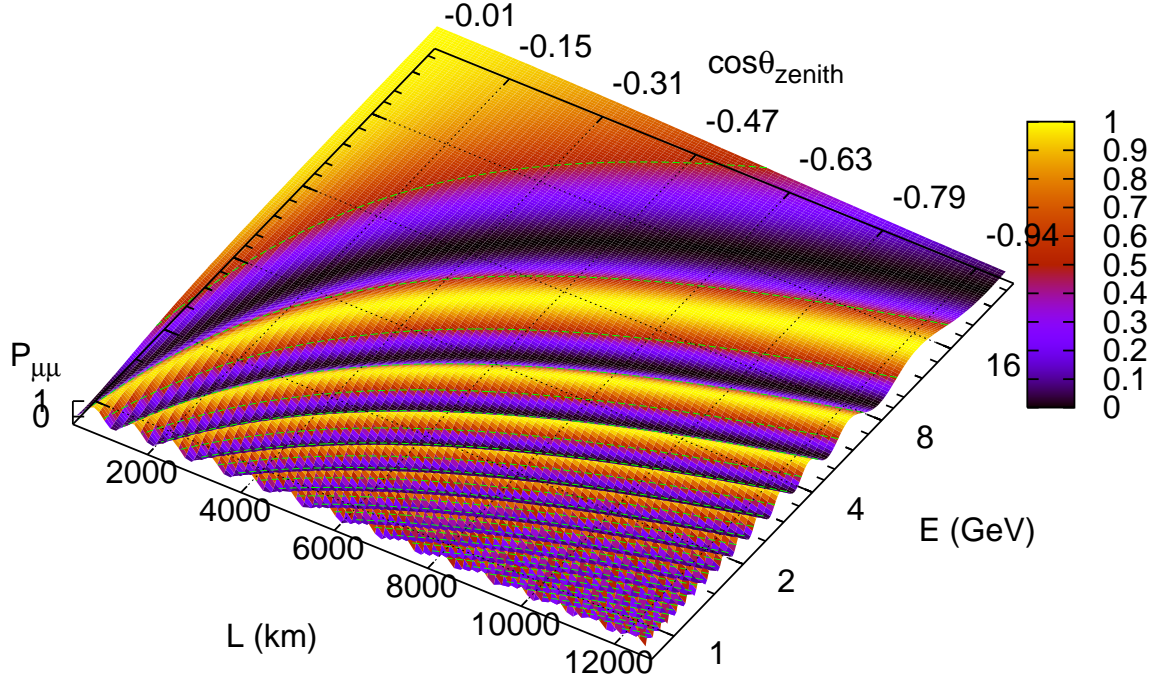


FIG. 2: The $\nu_\mu \rightarrow \nu_\mu$ oscillation probability in vacuum. We choose $\Delta m_{32}^2 = -2.5 \times 10^{-3} \text{eV}^2$, $\theta_{23} = 45^\circ$ and $\theta_{13} = 0^\circ$.

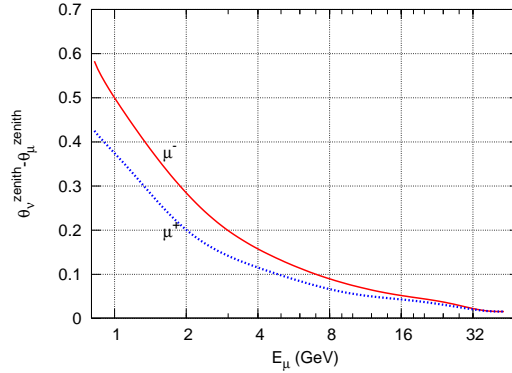


FIG. 3: The variation of the half width at half maxima with E_μ for the distribution of $\theta_\nu^{\text{zenith}} - \theta_\mu^{\text{zenith}}$ at horizon. The distribution is obtained for each E_μ bin from 500 years un-oscillated atmospheric data of 1 Mton ICAL.

distribution defined by the expression:

$$\chi^2 = \sum_{i,j=1}^{n_L, n_E} \left[2 \left\{ N_{ij}^p \left(1 + \sum_{k=1}^{n_s} f_{ij}^k \cdot \xi^k \right) - N_{ij}^o \right\} - 2N_{ij}^o \ln \left(\frac{N_{ij}^p \left(1 + \sum_{k=1}^{n_s} f_{ij}^k \cdot \xi_k \right)}{N_{ij}^o} \right) \right] + \sum_{k=1}^{n_s} \xi_k^2 \quad (7)$$

Here, N_{ij}^o is the number of observed events generated by Nuance for a given set of oscillation parameters with an exposure of 1 Mton.year of ICAL and N_{ij}^p is the number of predicted events (discussed later). These are obtained in a 2-dimensional grids in the plane of $\log E - L^{0.4}$. The term f_{ij}^k is the systematic uncertainty

of N_{ij}^p due to the k th uncertainty (discussed later) and ξ_k is the pull variable for the k th systematic uncertainty. We use total number of $\log E$ bins $n_E = 35$ (0.8 – 40 GeV) and the number of $L^{0.4}$ bins as a function of the energy. We consider $n_L = 2 \times 25, 2 \times 27, 2 \times 29, 2 \times 31,$ and 2×33 for $E = 0.8 - 1, 1 - 2, 2 - 3, 3 - 4,$ and > 4 GeV, respectively. For the down-going events, the binning is done by replacing ‘ $L^{0.4}$ ’ by ‘ $-L^{0.4}$ ’. The factor ‘2’ is taken to consider both up and down going cases. For the up going neutrino, L is the distance traveled by the neutrino from the source at the atmosphere to the detector in the underground. In case of the down going neutrino, the L is the ‘mirror L ’ which is the same L if the neutrino comes from exactly opposite direction.

The table of Honda flux is given in $20 \cos \theta_{\text{zenith}}$ bins and 101 E bins (0.1 – 10^4 GeV). It should be noted that we first re-binned the data into 300 $\cos \theta_{\text{zenith}}$ bins and 200 $\log E$ bins (0.8–40 GeV) to get the oscillation pattern accurately. This large number of $\cos \theta_{\text{zenith}}$ bins also help in proper re-binning of the data into $L^{0.4}$ bins.

A. Migration from neutrino to muon

To generate the theoretical data for the chi-square analysis, we first generate 500 years un-oscillated data for 1 Mton detector by Nuance. From this data we find the energy-angle correlated resolutions (see Figs. 4) in 35 E^ν bins (in log scale for the range of 0.8 – 40 GeV) and 17 $\cos \theta_{\text{zenith}}^\nu$ bins (for the range -1 to $+1$). For a given $\log E_\nu$ bin, we calculate the efficiency of having $E_\mu \geq 0.8$ GeV (threshold of the detector). For each set of oscillation parameters, we integrate the oscillated atmospheric neutrino flux folding the cross section, the exposure time, the target mass, the efficiency and the resolution function to obtain the predicted data. We use the CC cross section of Nuance-v3 [13] and the Honda flux in 3-dimensional scheme [18]. This method has been discussed in detail in [14], but the number of bins and resolution functions have been changed here.

One can do this directly by generating 500 Mton.year data (to ensure that the statistical error is negligible) for **each set** of oscillation parameters and then reducing it to 1Mton.year equivalent data, which would be the more straight forward method. The marginalization study with this method is almost an un-doable job in a normal CPU. However, an exactly equivalent result is obtained here using the energy-angle correlated resolution function.

We have done this study for ideal muon detector. From GEANT simulation of ICAL detector it is seen that the energy resolution of muon varies 4–10% depending on the direction and energy. Since the iron plates are stacked horizontally, the resolution will be better for vertical events than the slanted events. The angular resolution varies from 4–12% for the considered range of energy and zenith angle. Here, the thickness of iron plates are considered to be 6 cm. From Fig. 4 it is clear that these are negligible compared to the resolutions obtained from kinematics of scattering processes.

The addition of the hadron energy to the muon energy of an event, which might improve the reconstructed neutrino energy resolution, is not considered here for conservative estimation of the sensitivity. It would be realistic in case of GEANT-based studies since the number of hits produced by the hadron shower strongly depends on the thickness of iron layers. However, ICAL can also detect the neutral current events. Though it is expected that these events will not have any directional information; energy dependency of the oscillation, averaged over all directions can also contribute to the total χ^2 in the sensitivity studies separately.

B. Systematic uncertainties

The atmospheric neutrino flux is not known precisely, there are huge uncertainties in its estimation. We may divide them into two categories: I) overall uncertainties (which are independent of energy and zenith angle), and II) tilt uncertainties (which are dependent of energy and/or zenith angle). We consider the following types of uncertainties.

The energy dependent uncertainty, which arises due to the uncertainty in spectral indices, can be expressed as

$$\Phi_{\delta_E}(E) = \Phi_0(E) \left(\frac{E}{E_0} \right)^{\delta_E} \approx \Phi_0(E) \left[1 + \delta_E \log_{10} \frac{E}{E_0} \right]. \quad (8)$$

Similarly, the vertical/horizontal flux uncertainty as a function of zenith angle can be expressed as

$$\Phi_{\delta_z}(\cos \theta_z) \approx \Phi_0(\cos \theta_z) [1 + \delta_z (|\cos \theta_z| - 0.5)]. \quad (9)$$

Next, we consider the overall flux normalization uncertainty δ_{f_N} , and the overall neutrino cross section uncertainty δ_σ .

For $E < 1$ GeV we consider $\delta_E = 5\%$ and $E_0 = 1$ GeV and for $E > 10$ GeV, $\delta_E = 5\%$ and $E_0 = 10$ GeV.

We take $\delta_{f_N} = 10\%$, $\delta_\sigma = 15\%$. We consider $\delta_z = 4\%$ which leads to 2% vertical/horizontal flux uncertainty. We derived these uncertainties from [24].

For each set of oscillation parameters, we calculate the χ^2 in two stages. First we used ξ_k such that $\frac{\delta\chi^2}{\delta\xi_k} = 0$, which can be obtained solving the equations [27]. Then we calculate the final χ^2 with these ξ_k values. Finally, we minimize the χ^2 with respect to all oscillation parameters [29].

VII. MARGINALIZATION AND RESULTS

A global scan of χ^2 is carried out over the oscillation parameters Δm_{32}^2 , θ_{23} , θ_{13} and δ_{CP} with neutrinos and anti-neutrinos separately. We have chosen the range of $|\Delta m_{32}^2| = 2.0 - 3.0 \times 10^{-3} \text{eV}^2$, $\theta_{23} = 38^\circ - 52^\circ$, $\theta_{13} = 0^\circ - 12.5^\circ$ and $\delta_{CP} = 0^\circ - 360^\circ$. The 2-dimensional 68%, 90%, 99% confidence level allowed parameter spaces (APSs) are obtained by considering $\chi^2 = \chi_{\text{min}}^2 + 2.48, 4.83, 9.43$, respectively. For every set of data we have checked that chi-square/d.o.f remains $\lesssim 1.1$ at its minimum value. We obtain the APS in $|\Delta m_{32}^2| - \theta_{23}$ and $|\Delta m_{32}^2| - \theta_{13}$ plane. We set the input of $|\Delta m_{32}^2| = 2.5 \times 10^{-3} \text{eV}^2$ and $\delta_{CP} = 0$.

It is important to note here that the statistics changes significantly over $L - E$ plane with the change of oscillation parameters. Moreover, the fluxes and the resolutions are very different at different $L - E$ zones. The upper and lower bounds of an oscillation parameter depends significantly on the statistics as well as on the resolutions of the specific zones in $L - E$ plane. The binning of the data, which captures the oscillation patten also plays the vital role.

However, for some sets of input parameters the chi-square remains almost flat over a significant range of a parameter and then changes rapidly. It happens due to the fact that I) the change of oscillation probability is insignificant, and/or II) the above change is significant, but it is eaten by the systematic uncertainties in chi-square analysis. In this circumstances, the best-fit values may change significantly from the input values. This is a very common feature in analyses with generating events by Monte Carlo method. But, in methods without Monte Carlo, the number of events are determined with an accuracy of a fraction of 1 and then best-fit values is always close to the input values.

In some cases, the deviations of the best-fit values are large. This is happened due to the following reasons. Here, we have just folded the total charge current

cross section of all processes to find the number events for a particular neutrino energy to generate the theoretical data. We see significant fluctuations more than 1 σ in number of events between ‘‘theoretical data’’ and ‘‘experimental data’’ in some particular energy bins for a given set of oscillation parameters (see Fig. 5). This happens mainly at the neutrino energy $\lesssim 3$ GeV, where the resonances occur. Here, the neutrino cross sections depend on the type of nucleus. The generation of events is very complicated here and it depends on the models. These all are not considered in the same way as in Nuance in generation of theoretical data, which causes energy dependent systematic uncertainty. However, this has no regular pattern. In our analysis we consider only the over all uncertainty in the cross section. These energy dependent uncertainties have not been considered in our analysis. When θ_{23} deviates from $\pi/4$, the difference between peak and dip decreases and the fluctuations becomes relatively prominent. Again, when θ_{13} becomes large, the periodic pattern of oscillation is lost due to matter effect. We have checked that the fluctuations are larger for $\theta_{23} = 50^\circ$ and $\theta_{13} = 7.5^\circ$ than $\theta_{23} = 45^\circ$ and $\theta_{13} = 0^\circ$. In this region of oscillation parameters, significant deviations of best-fit values of oscillation parameters from their true values are obtained.

The variation of $\Delta\chi^2 [= \chi^2 - \chi_{\text{min}}^2]$ with each of θ_{23} , θ_{13} and Δm_{32}^2 , are shown in Fig. 6, 7, 8, and 9. These are after marginalization over all the oscillation parameters except one, with which it varies. We present the cases for inputs $\theta_{13} = 0^\circ$, and 7.5° with $\theta_{23} = 40^\circ, 45^\circ$, and 50° , respectively.

A. Sensitivity to θ_{23} and its octant discrimination

As the present experiments indicate that the value of θ_{13} is small compared to θ_{23} , the atmospheric neutrino oscillation is mainly governed by two flavor oscillation $\nu_\mu (\bar{\nu}_\mu) \leftrightarrow \nu_\tau (\bar{\nu}_\tau)$. This constrains $\sin^2 2\theta_{23}$ and $|\Delta m_{32}^2|$.

From Fig. 10, we see that the deviation from the maximal mixing between **2** and **3** flavor eigen states can be observed. However, a degeneracy in θ_{23} arises in case of $\theta_{13} = 0$, whether it is larger or smaller than 45° . But, when the matter effect comes into the play, a resonance occurs in $\nu_\mu (\bar{\nu}_\mu) \leftrightarrow \nu_e (\bar{\nu}_e)$ oscillation and it leads to a large effective value of θ_{13} (see Eq. 4). This helps to dominate the $\sin^4 \theta_{23}$ term in Eq. 3 and breaks the θ_{23} degeneracy in its measurement. Since the atmospheric neutrinos cover a large region of $E - L$ plane, it can ob-

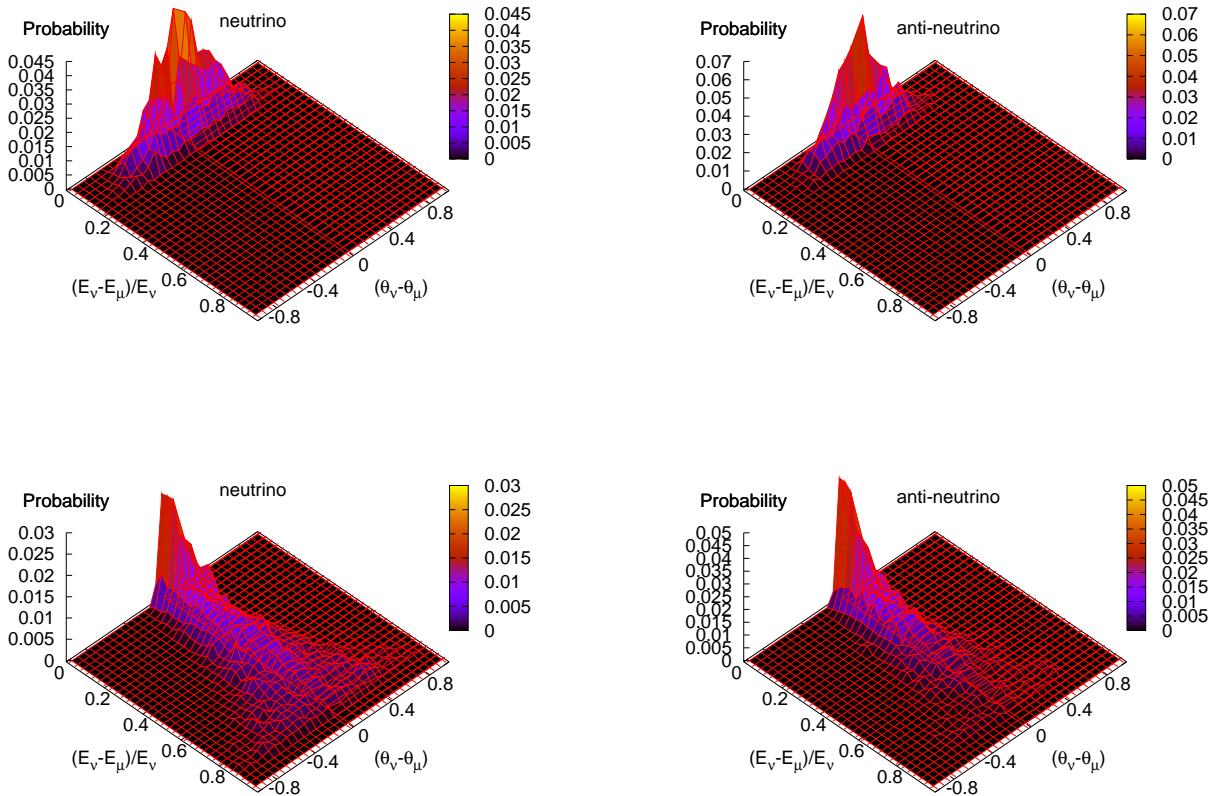


FIG. 4: The sample energy-angle correlated resolution plots for neutrino (left column) and anti-neutrino (right column) for the bins of $E_\nu = 0.85 - 0.98$ GeV with $\cos \theta_{\text{zenith}} = -0.40$ to -0.20 (upper row) and $E_\nu = 6.84 - 7.86$ GeV with $\cos \theta_{\text{zenith}} = 0$ to 0.20 (lower row). The data is obtained from the simulation of 500 Mton.year exposure of ICAL considering no oscillation.

serve the matter resonance and has an ability to discriminate the octant degeneracy. In Fig. 6, the variations of $\Delta\chi^2 = (\chi^2 - \chi_{\text{min}}^2)$ with θ_{23} are shown for input values of $\theta_{23} = 40^\circ$, 45° and 50° with $\theta_{13} = 0^\circ$ and 7.5° , respectively. We see that with increase in θ_{13} , the matter effect not only discriminates the octant, but increases the precision also.

In Fig. 10 we see that for $\theta_{13} = 7.5^\circ$ the octant discrimination is possible for input of $\theta_{23} = 40^\circ$ and 50° with IH. But it is not possible for NH. Normally, the flux of ν_μ is higher than $\bar{\nu}_\mu$. In case of IH (NH), $\bar{\nu}_\mu$ (ν_μ) is suppressed. The statistics remains high for IH compared to NH, which leads better octant discrimination possibility for IH.

B. Sensitivity to θ_{13}

The effect of θ_{13} in oscillation probability does not appear dominantly neither in atmospheric nor in solar neutrino oscillation, but as a subleading in both oscillations. In case of atmospheric neutrino, its effect is seen at a) $E \sim 1$ GeV for propagation of neutrinos through vacuum as well as through matter (no matter resonance), and b) $E \approx 2 - 10$ GeV for propagation only through matter (matter resonance). The matter effect enhances the difference in oscillation probabilities between two θ_{13} values for neutrinos with NH and for anti-neutrinos with IH (see Eq. 4). In Fig. 7 we show the cases a) and b) considering neutrinos and anti-neutrinos separately. We find that the effect of case a) is negligible.

We have plotted the APS in $\theta_{13} - |\Delta m_{32}^2|$ plane in Fig 11 for $\theta_{13} = 0^\circ$, 5° , and 7.5° with $\theta_{23} = 40^\circ$, 45° and 50° , respectively. We find that the matter effect significantly

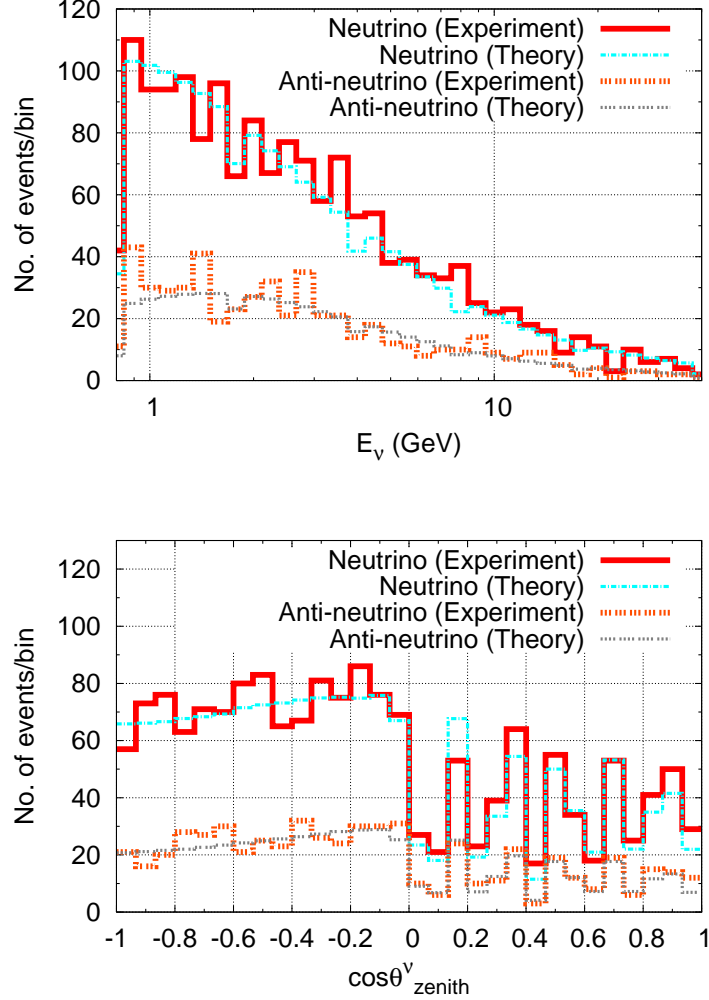


FIG. 5: The typical distribution of events with E_ν , keeping $\cos\theta_{\text{zenith}}^\nu$ fixed at ≈ -0.367 and with $\cos\theta_{\text{zenith}}^\nu$ keeping E_ν fixed at ≈ 2.24 GeV. We set $\Delta m_{32}^2 = -2.5 \times 10^{-3} \text{eV}^2$, $\theta_{23} = 45^\circ$, $\theta_{13} = 0^\circ$ and $\delta_{CP} = 0^\circ$.

constrains θ_{13} over the present limit. Though the matter effect acts either on neutrinos or on anti-neutrinos depending on the type of the hierarchy, but we have checked that it improves when we consider both neutrinos and anti-neutrinos. The sensitivity of θ_{13} is not generally expected to be improved for the case of analysis with neutrinos and anti-neutrinos in together. However, this happens here due to the marginalization which restricts θ_{23} more tightly for the case of ν and $\bar{\nu}$ in together than either with ν or $\bar{\nu}$ and indirectly constrains θ_{13} . It is also seen that the APS is strongly dependent on the input of θ_{23} and a better constraint is obtained for $\theta_{23} > 45^\circ$. However, it is notable here that the uncertainty is very high and the best-fit values deviate largely from its input values for nonzero θ_{13} inputs due to the reasons discussed

at the beginning of this section.

C. Sensitivity to Δm_{32}^2

We show the constraint on $|\Delta m_{32}^2|$ in Fig. 10 and 11. We see that the precision is little better when $\theta_{13} = 0$. The reason behind this is that a regular oscillation pattern with periodic rise and fall is observed when $\theta_{13} = 0$.

It is seen that the APS is larger for NH than IH. The matter effect does not act on neutrino for IH and anti-neutrinos for NH with an addition to the fact that the flux is higher for neutrino than anti-neutrino. As discussed above, the APS is more restricted when there is no matter effect. Here, for input with IH the number of neutrino events is high and they do not have any matter effect.

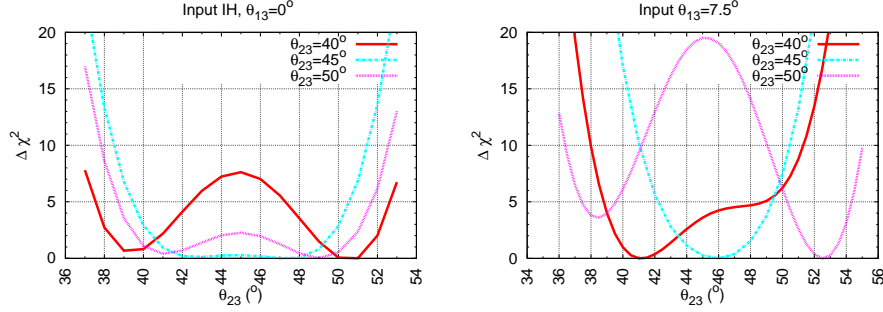


FIG. 6: The variation of $\Delta\chi^2 = (\chi^2 - \chi_{\min}^2)$ with θ_{23} for input value of $\theta_{23} = 40^\circ$, 45° and 50° with $\theta_{13} = 0^\circ$ and $\theta_{13} = 7.5^\circ$, respectively. Here, we consider both neutrinos and anti-neutrinos together. The type of input hierarchy is inverted.

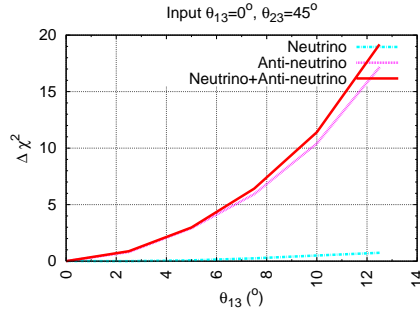


FIG. 7: The variation of $\Delta\chi^2 = (\chi^2 - \chi_{\min}^2)$ with θ_{13} for input value of $\theta_{13} = 0^\circ$, and $\theta_{23} = 45^\circ$ considering neutrino, anti-neutrino and both types of neutrinos, respectively.

This leads to smaller APS for IH compared to NH for large values of θ_{13} .

D. Effect of events at near horizon on precision measurements

For a given set of input parameters, if we compare the APSs with zenith angle cut (discussed in section V) with those without any cut, we find no significant differences. As a demonstrating example, we have shown the APSs in Fig. 12 without imposing any zenith angle cut for a given set of oscillation parameters. One can find the corresponding plots with zenith angle cut in Figs. 10 and 11.

From the study of this paper, we can conclude that the events at near horizon cannot contribute significantly in precision measurements. The fact is that the L resolution is very poor here. A little change in zenith angle at near horizon changes L values drastically. Again, the discrimination of up and down going events are not possible. So, the oscillation effect is almost smeared out by the resolutions. From the L/E dip considering the L and E values of neutrinos, one can expect a large contribution

in precision from these events. But, in practical situation, there is no appreciable improvement after addition of these events.

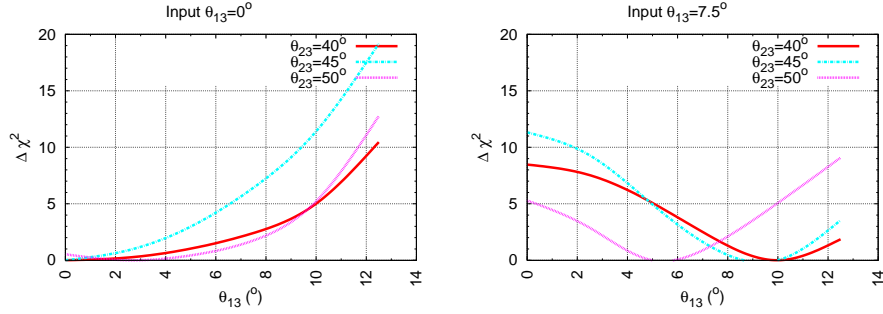
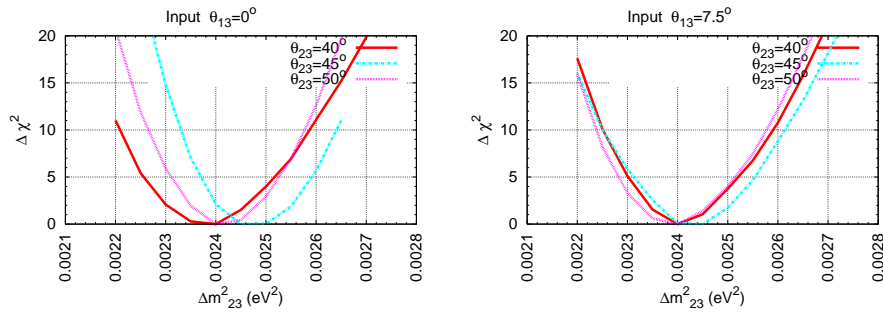
The vertical (horizontal) stacking of iron plates will be able to detect the horizontal (vertical) events. So, from this study one can conclude that horizontal stacking is expected to give better precision than the vertical stacking.

E. Precision of the parameters

For a quantitative assessment of the result, we define the precision of a parameter t as:

$$P = 2 \left(\frac{t^{\max} - t^{\min}}{t^{\max} + t^{\min}} \right). \quad (10)$$

We find that the precisions are strongly dependent on the set of input parameters. We obtained the precision of $|\Delta m_{32}^2| \approx 6.4\%$, 8.8% and 12% at 68%, 90% and 99% CL, respectively and the precision of $\sin^2 \theta_{23} \approx 31\%$, 38% , and 41% at 68%, 90% and 99% CL, respectively for the input of $\theta_{23} = 45^\circ$ and $\theta_{13} = 0^\circ$.

FIG. 8: The same as Fig. 6, but with θ_{13} .FIG. 9: The same as Fig. 6, but with Δm_{32}^2 .

The oscillation dip moves towards the lower L/E values as $|\Delta m_{32}^2|$ increases. The statistics also decreases at the lower L/E region. So, the precision is expected to be weaker as the input of $|\Delta m_{32}^2|$ increases.

A comparison of the precisions of Δm_{32}^2 and $\sin^2 \theta_{23}$ among different future baseline experiments is made in [28]. The variation of the precisions with the change of input parameters are also presented there. We compare our results with 5 years run of T2K, which is the best in determining precision of atmospheric oscillation parameters in the list in [28]. The precision of Δm_{32}^2 is almost same with T2K ($\approx 12\%$) and precision of $\sin^2 \theta_{23}$ from ICAL is 41% while from T2K is 46%. Here we present the results for 10 years run of 100 kTon ICAL detector. From this work it is also seen that atmospheric neutrinos at ICAL detector are in very good position to discriminate octant of θ_{23} . The main advantage here is that atmospheric neutrinos are natural sources and the cost goes only to build and run the detector.

VIII. CONCLUSION

We have studied the precisions of the oscillation parameters from atmospheric neutrino oscillation experi-

ment at the large magnetized ICAL detector generating events by Nuance and considering only the muons produced by the charge current interactions. The distance between two consecutive peaks of oscillation in E for fixed L increases as one goes from higher L values to its lower values. This indicates the need of finer binning at lower L values in χ^2 analysis. We optimize the binning of the data in the grids of $\log E - L^{0.4}$ plane. We find that the impact of the events at near horizon on the precision measurements is very negligible due to poor L resolution.

From the marginalized χ^2 study separately for neutrinos and anti-neutrinos, we find that the measurement of θ_{13} is possible at a considerable precision with atmospheric neutrinos. The precision of θ_{13} depends crucially on its input value. For $\theta_{13} = 0$, we find its upper bound $\approx 4^\circ$, 6° and 9° at 68%, 90% and 99% CL, respectively. The both lower and upper bounds of θ_{13} are also possible for some combinations of $(\theta_{23}, \theta_{13})$ and it happens mainly for $\theta_{23} \gtrsim 45^\circ$.

The precision of $|\Delta m_{32}^2|$ and θ_{23} can also be very high and the determination of octant of θ_{23} is possible for some combinations of $(\theta_{23}, \theta_{13})$.

It should also be noted here that in χ^2 analysis the theoretical data and the experimental data are not generated in the same way. The different models of neutrino

interactions generate energy dependent systematic uncertainties at some energies. These are not included in this analysis. This causes sometimes large deviation of the best-fit values of the oscillation parameters from the input values.

Acknowledgments: This research has been sup-

ported by funds from Neutrino Physics projects at HRI. The use of excellent cluster computational facility installed from this project is gratefully acknowledged. A part of the computation was also carried out in HRI general cluster facility.

-
- [1] G. L. Fogli *et al.*, Phys. Rev. D **78**, 033010 (2008) [arXiv:0805.2517 [hep-ph]].
- [2] R. N. Mohapatra and W. Rodejohann, Phys. Rev. D **72**, 053001 (2005) [arXiv:hep-ph/0507312].
- [3] R. N. Mohapatra *et al.*, Rept. Prog. Phys. **70**, 1757 (2007) [arXiv:hep-ph/0510213].
- [4] J. Escamilla, D. C. Latimer and D. J. Ernst, Phys. Rev. Lett. **103**, 061804 (2009) [arXiv:0805.2924 [nucl-th]].
- [5] J. E. Roa, D. C. Latimer and D. J. Ernst, arXiv:0904.3930 [nucl-th].
- [6] C. K. Jung, AIP Conf. Proc. **533**, 29 (2000) [arXiv:hep-ex/0005046].
- [7] Y. Itow *et al.* [The T2K Collaboration], arXiv:hep-ex/0106019.
- [8] D. S. Ayres *et al.* [NOvA Collaboration], arXiv:hep-ex/0503053.
- [9] K. Nakamura, Int. J. Mod. Phys. A **18**, 4053 (2003).
- [10] V. Arumugam *et al.* [INO Collaboration], INO-2005-01.
- [11] S. Choubey and P. Roy, Phys. Rev. D **73**, 013006 (2006) [arXiv:hep-ph/0509197].
- [12] D. Indumathi, M. V. N. Murthy, G. Rajasekaran and N. Sinha, Phys. Rev. D **74**, 053004 (2006) [arXiv:hep-ph/0603264].
- [13] D. Casper, Nucl. Phys. Proc. Suppl. **112**, 161 (2002) [arXiv:hep-ph/0208030].
- [14] A. Samanta, Phys. Lett. B **673**, 37 (2009) [arXiv:hep-ph/0610196].
- [15] A. Samanta, Phys. Rev. D **79**, 053011 (2009) arXiv:0812.4640 [hep-ph].
- [16] T. Maeno *et al.* [BESS Collaboration], Astropart. Phys. **16**, 121 (2001) [arXiv:astro-ph/0010381].
- [17] J. Alcaraz *et al.* [AMS Collaboration], Phys. Lett. B **461**, 387 (1999) [arXiv:hep-ex/0002048].
- [18] M. Honda, T. Kajita, K. Kasahara and S. Midorikawa, Phys. Rev. D **70**, 043008 (2004) [arXiv:astro-ph/0404457].
- [19] Y. Ashie *et al.* [Super-Kamiokande Collaboration], Phys. Rev. D **71**, 112005 (2005) [arXiv:hep-ex/0501064].
- [20] Y. Ashie *et al.* [Super-Kamiokande Collaboration], Phys. Rev. Lett. **93**, 101801 (2004) [arXiv:hep-ex/0404034].
- [21] S. P. Mikheev and A. Y. Smirnov, Sov. J. Nucl. Phys. **42**, 913 (1985) [Yad. Fiz. **42**, 1441 (1985)]; Nuovo Cim. C **9**, 17 (1986).
- [22] L. Wolfenstein, Phys. Rev. D **17**, 2369 (1978).
- [23] C. Giunti, C. W. Kim and M. Monteno, Nucl. Phys. B **521**, 3 (1998) [arXiv:hep-ph/9709439].
- [24] M. Honda, T. Kajita, K. Kasahara, S. Midorikawa and T. Sanuki, Phys. Rev. D **75**, 043006 (2007) [arXiv:astro-ph/0611418].
- [25] H. Nunokawa, S. J. Parke and R. Zukanovich Funchal, Phys. Rev. D **72**, 013009 (2005) [arXiv:hep-ph/0503283].
- [26] A. de Gouvea, J. Jenkins and B. Kayser, Phys. Rev. D **71**, 113009 (2005) [arXiv:hep-ph/0503079].
- [27] G. L. Fogli, E. Lisi, A. Marrone, D. Montanino and A. Palazzo, Phys. Rev. D **66**, 053010 (2002) [arXiv:hep-ph/0206162].
- [28] P. Huber, M. Lindner, M. Rolinec, T. Schwetz and W. Winter, Nucl. Phys. Proc. Suppl. **145**, 190 (2005) [arXiv:hep-ph/0412133].
- [29] Here, we consider all uncertainties as a function of reconstructed neutrino energy and zenith angle. Here we assumed that the tilt uncertainties will not be changed too much due to reconstruction. However, on the other hand if any tilt uncertainties arises in reconstructed neutrino events from the reconstruction method or the kinematics of the scattering, it is then accommodated in χ^2 .

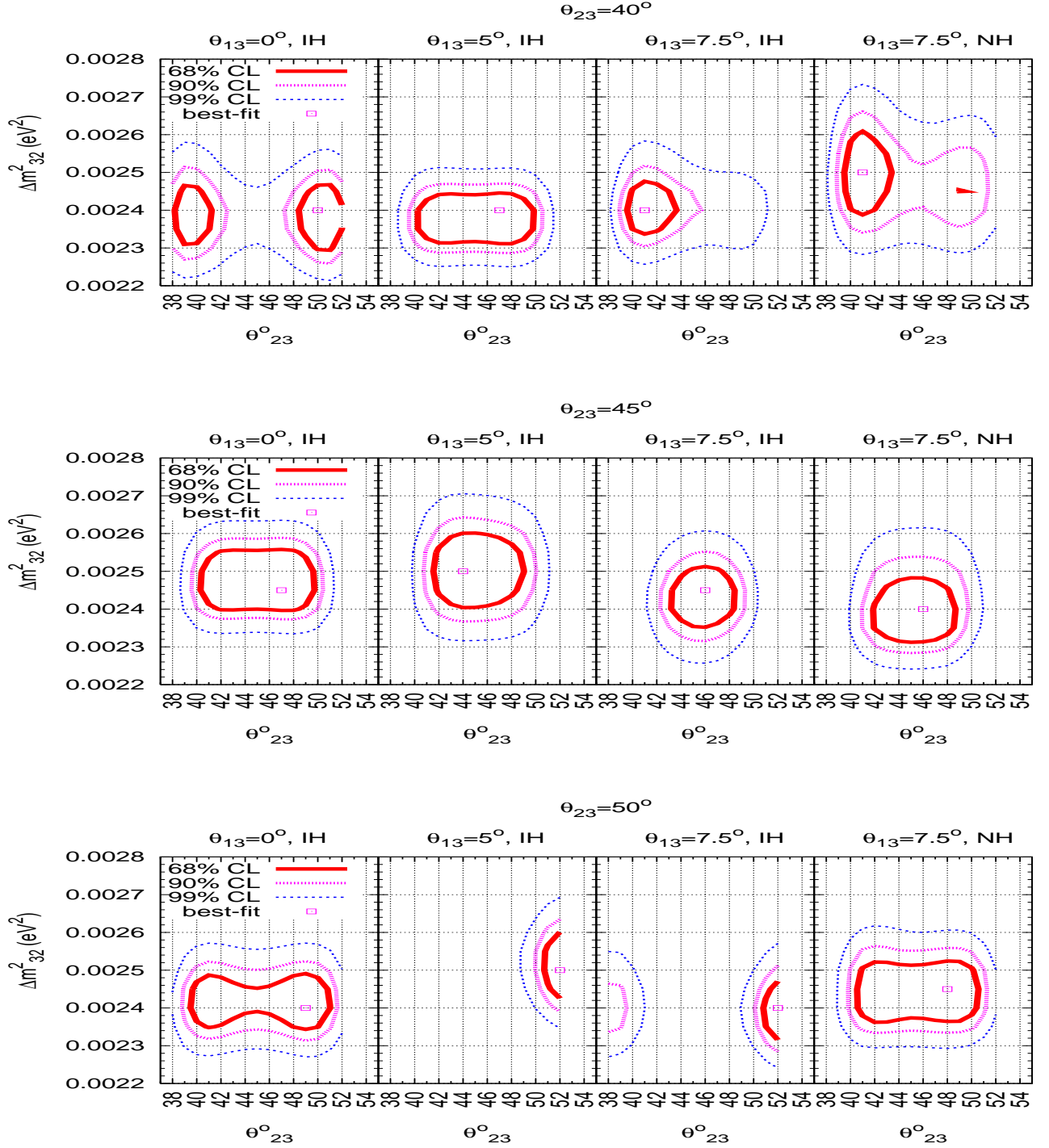


FIG. 10: The 68%, 90%, 99% CL allowed regions in $\theta_{23} - |\Delta m_{32}^2|$ plane for the input of $\theta_{23} = 40^\circ$ (first row), 45° (second row), 50° (third row) with $\theta_{13} = 0^\circ$ (first column), 5° (second column), 7.5° (third column) with IH and 7.5° (fourth column) with NH.

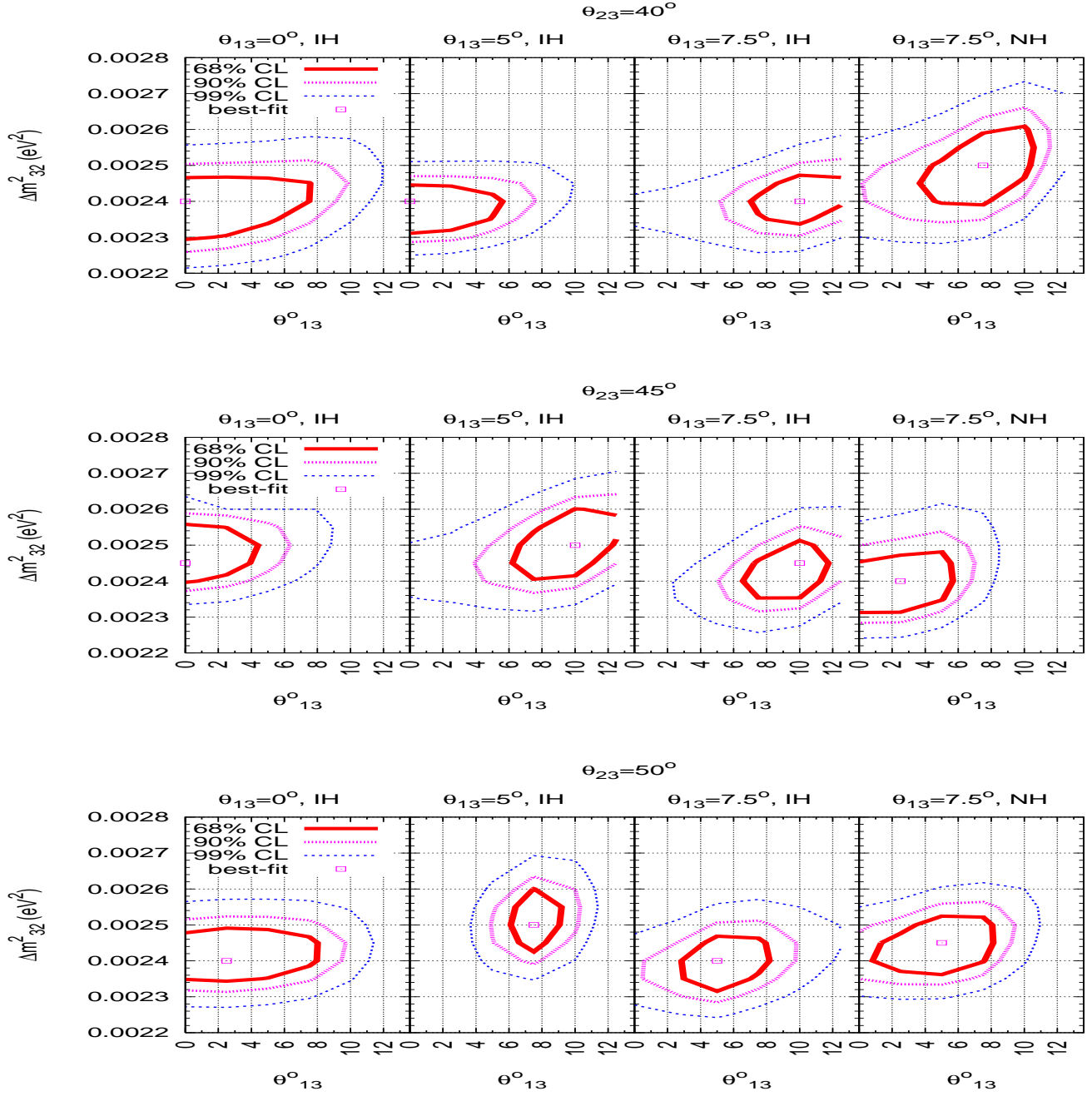


FIG. 11: The same as Fig. 10, but in $\theta_{13} - |\Delta m_{32}^2|$ plane.

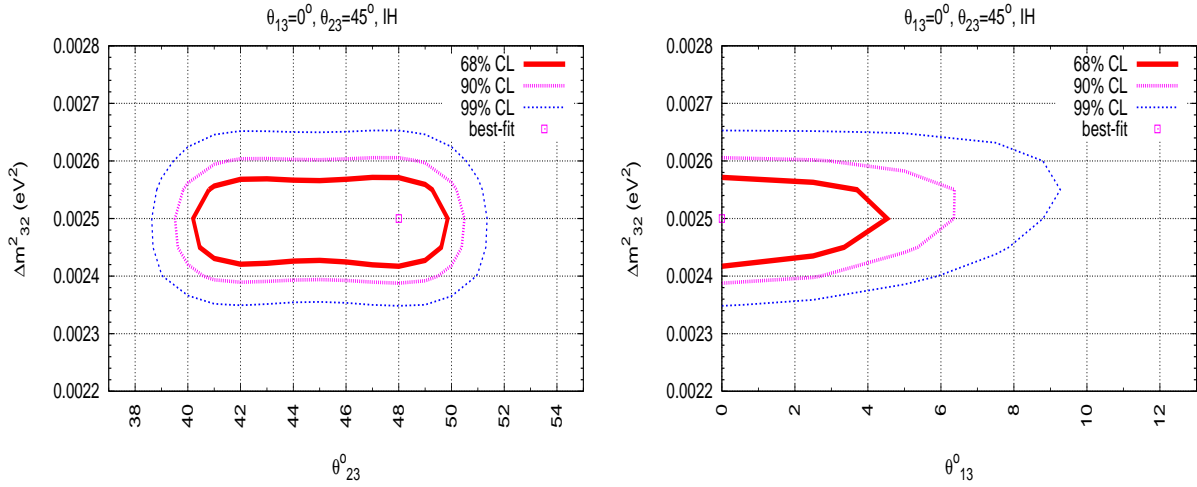


FIG. 12: The allowed regions without any zenith angle cut for the events at the horizon.